RESEARCH ARTICLE | OCTOBER 18 2024

Neural network–enabled, all-electronic control of non-Newtonian fluid flow **⑤ ⑥ ⊘**

Huilu Bao 💿 ; Xin Zhang 💿 ; Xiaoyu Zhang 💿 ; Xiao Fan 💿 ; J. William Boley 💿 ; Jinglei Ping 🗷 💿



Appl. Phys. Lett. 125, 164105 (2024) https://doi.org/10.1063/5.0226525

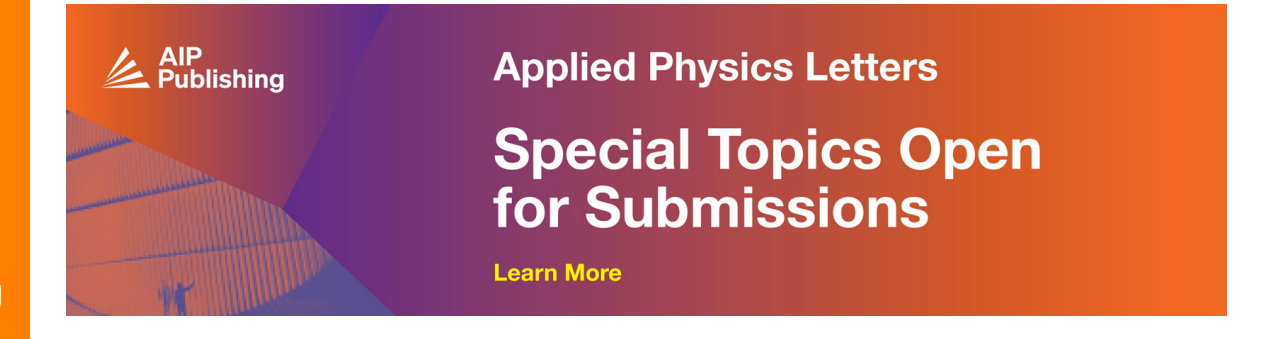




Articles You May Be Interested In

Electrical contactless microfluidic flow quantification

Appl. Phys. Lett. (January 2022)





Neural network-enabled, all-electronic control of non-Newtonian fluid flow (1) (s)

Cite as: Appl. Phys. Lett. **125**, 164105 (2024); doi: 10.1063/5.0226525 Submitted: 2 July 2024 · Accepted: 17 September 2024 · Published Online: 18 October 2024









AFFILIATIONS

- Department of Mechanical and Industrial Engineering, University of Massachusetts Amherst, Amherst, Massachusetts 01003, USA
- ²Department of Mechanical Engineering, Boston University, Boston, Massachusetts 02215, USA
- ³Division of Materials Science and Engineering, Boston University, Boston, Massachusetts 02215, USA

ABSTRACT

Real-time, all-electronic control of non-Newtonian fluid flow through a microscale channel is crucial for various applications in manufacturing and healthcare. However, existing methods lack the sensitivity required for accurate measurement and the real-time responsiveness necessary for effective adjustment. Here, we demonstrate an all-electronic system that enables closed-loop, real-time, high-sensitivity control of various waveforms of non-Newtonian fluid flow $(0.76 \, \mu \text{l min}^{-1})$ through a micro-sized outlet. Our approach combines a contactless, cuff-like flow sensor with a neural-network control program. This system offers a simple, miniaturized, versatile, yet high-performance solution for non-Newtonian fluid flow control, easily integrated into existing setups.

Published under an exclusive license by AIP Publishing. https://doi.org/10.1063/5.0226525

Controlling the flow rate of non-Newtonian fluid is crucial in various fields, including food production, 1,2 manufacturing, 3,4 and healthcare. 5,6 All-electronic flow control offers high compatibility in industrialization and provides significant promise for miniaturization, low cost, and speed. However, the dependence of viscosity on stress⁷ presents substantial challenges for accurate real-time, all-electronic control of non-Newtonian flow rates, especially through a micro-sized outlet where flow geometry and conditions often vary spatially. Typical techniques often fall short in both flow sensing and adjustment. Conventional ultrasonic flow meters⁸ are bulky and can have inaccuracies of up to 18%. Coriolis flow meters 10,11 offer high accuracy for low-viscosity non-Newtonian fluids but are costly, large, and cause considerable disturbance to the measured flow. 12 Additionally, these methods, along with techniques reliant on computer vision monitoring, 13-15 face challenges in integrating with existing setups and implementing flow rate quantification at a micro-sized fluidic outlet. For flow adjustment, the widely used proportional-integral-derivative (PID) controller 16,17 is not fully automatic and is less effective for nonlinear flows, such as those of non-Newtonian fluids, particularly when the flow measurement is subject to unknown disturbances. 18-

Here, we develop an all-electronic system for real-time, closed-loop control of non-Newtonian fluid flow. This system comprises an electrical flow sensor and an artificial-intelligence (AI) flow-adjustment

algorithm, as shown in Fig. 1. The flow sensor operates on a contactless flow-sensing principle, 21 using a cuff-like transducer that wraps around the tip of the fluid dispensing nozzle (see the supplementary material—Methods section for details). The flow-adjustment algorithm, based on a radial basis function neural network (RBFNN), is capable of real-time analysis and feedback 22,23 and is suitable for controlling non-Newtonian fluids compared to other algorithms (see the supplementary material—Methods section for details). Our system delivers precise control of non-Newtonian fluids of various waveforms. The flow control accuracy is $0.76\,\mu l\, {\rm min}^{-1}$, meeting the requirements of most applications such as 3D printing, 24 drug delivery, 25 and artificial organs. 6

In our system, the flow rate of epoxy resin with a viscosity of $1600\,\mathrm{cP}$ is set by a syringe pump with an electronic interface (Fig. 1). As shown in Fig. 2(a), the flow rates (without flow control), determined using a gravimetric method, deviate significantly from the flow rates set on the syringe pump with a step waveform. The shear-thinning phenomenon is observed in the experiment, as reflected by the spikes in the data. The gravimetrically measured flow rate vs set flow rate plot [Fig. 2(b)] demonstrates a maximal deviation of $107\% \pm 1\%$, reflecting the nonlinearity of the epoxy resin flow. ²⁶ In contrast, the flow rate of water, a Newtonian fluid, matches the pump flow rate. ²¹

Our contactless flow sensor is based on a copper-tape transducer (3 mm in width) that wraps around a nozzle tip and connects to a

Institute of Applied Life Sciences, University of Massachusetts Amherst, Amherst, Massachusetts 01003, USA

a) Author to whom correspondence should be addressed: ping@engin.umass.edu

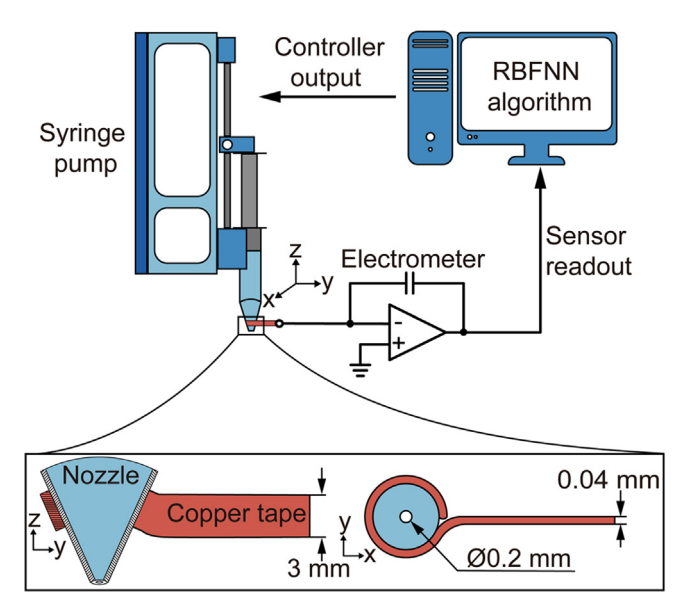


FIG. 1. Closed-loop non-Newtonian fluid flow rate control system. The electrometer is based on an operational amplifier with a feedback capacitor. The flow-adjustment algorithm is based on a radial basis function neural network (RBFNN).

coulomb meter, as shown in Fig. 1. The triboelectric interaction between the flowing fluid and the tip generates electric potential variations detected by the coulomb meter. The time-dependent electric current for the set step waveform is derived, as shown in Fig. 2(a), by

taking the time derivative of the coulometric measurement results over time for the epoxy resin flow (supplementary material, Fig. S1). The results show a clear association between the sensor current and the gravimetrically measured flow rate over time. As shown in Fig. 2(c), the sensor current for each flow rate, extracted from Fig. 2(a), depends linearly on the gravimetrically measured flow rate ($R^2 = 0.99$). Therefore, the sensor current is highly characteristic of the flow rate through the linear relationship (the calibration curve), with a sensitivity of 0.018 pA min μ l⁻¹ (slope of the linear response vs flow rate data) and a resolution of 0.76 μ l min⁻¹ (determined by dividing the noise level by the sensitivity).

Flow rates, determined by real-time current signal from the flow sensor and the linear current–flow rate relationship, are fed into the RBFNN-based flow-adjustment algorithm. As shown in Fig. 3(a), the neural network has three primary layers: the input layer, the hidden layer, and the output layer. The input layer receives the target flow rate (reference flow rate), r, and the coulometrically measured flow rate, y, to generate an input vector x with four components: r_t , y_t , r_{t-1} , and y_{t-1} , representing the most recent and previous target and measured flow rates. The hidden layer consists of neurons that apply Gaussian functions to x and performs weighted sum calculations to deliver an output signal, u, in the output layer, to control the speed of the syringe pump. This closed-loop control process continues iteratively, with an analysis time of ~ 2 ms per data point.

We use the system that incorporates the contactless flow sensor and the neural-network algorithm (see the supplementary material—Methods section for details) to control three epoxy flow waveforms: the step flow waveform [Fig. 2(a)] from 40 to 300 μ l min⁻¹, a sinusoidal flow waveform [Fig. 3(b)] oscillating between 20 and 320 μ l min⁻¹

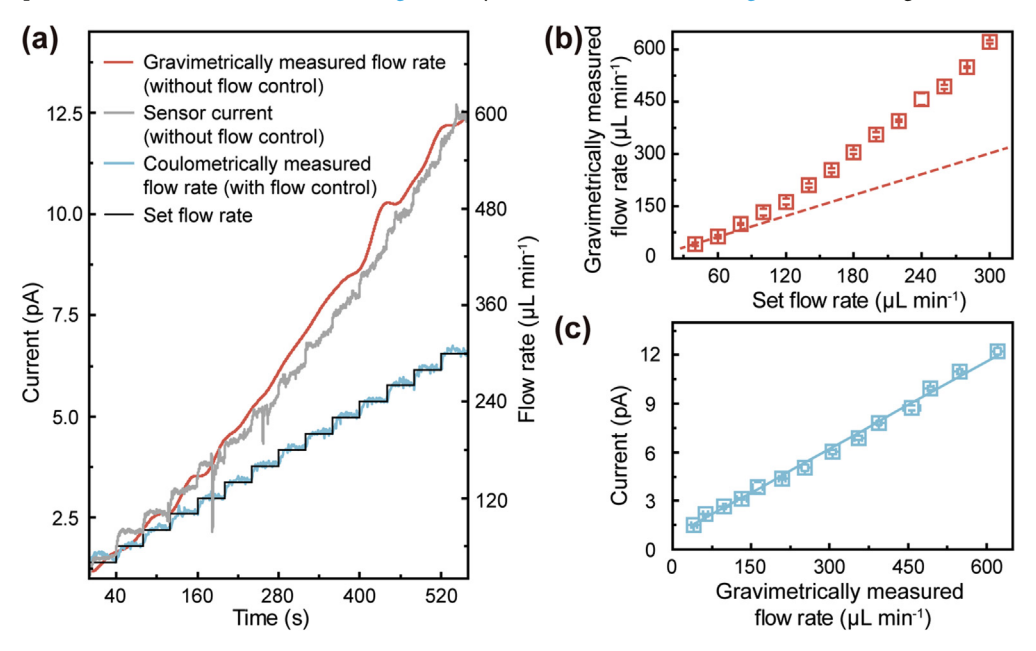


FIG. 2. Flow sensor response to varying flow rates of epoxy resin. (a) Current and flow rate over time for a step flow rate waveform set by the syringe pump. In the flow control experiment, the target waveform for the control program matches the set step waveform. (b) Gravimetrically measured flow rate (without flow control) vs syringe-pump set flow rate. The flow rate is averaged within the middle 20 s of each step in the waveform. The eye-guiding dashed line indicates the response of the Newtonian fluid's flow rate. Error bars represent the standard deviation. (c) Sensor current response as a function of the gravimetrically measured flow rate, without flow control. The blue line is the best linear fit to the data. The current is derived by averaging the current within the middle 20 s of each step in the waveform in (a). Horizontal and vertical error bars represent the standard deviations in the measurements for the gravimetrically measured flow rate and the sensor current, respectively.

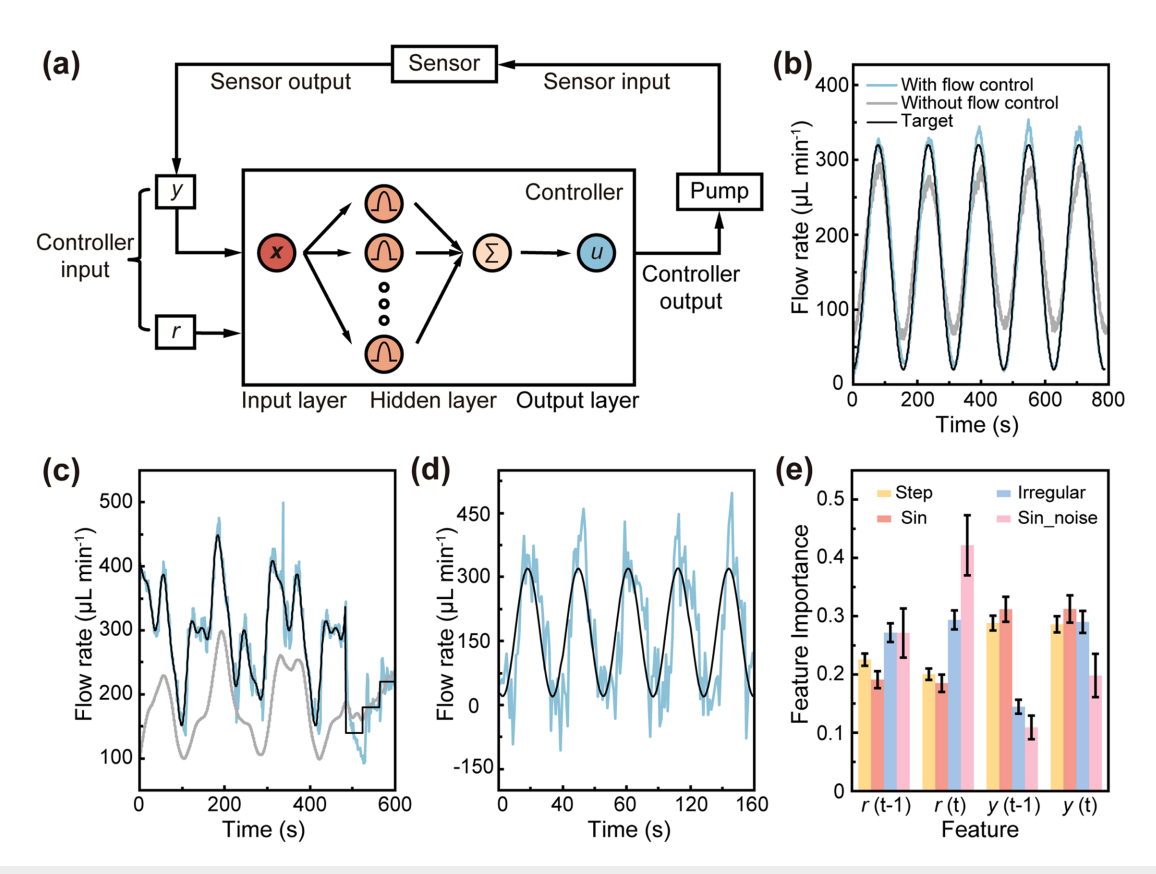


FIG. 3. Flow control based on a radial basis function neural network (RBFNN). (a) RBFNN algorithm diagram. (b) Coulometrically measured flow rate controlled by the closed-loop control system with a sinusoidal target flow waveform, in comparison to the uncontrolled, gravimetrically measured flow rate with the syringe pump set to match the target flow waveform. (c) Comparison for a random target flow waveform. (d) Coulometrically measured flow rate controlled by the closed-loop control system with a sinusoidal target flow waveform at the presence of artificial digital noise. Data in (b)–(d) use the same color code defined in (b). (e) Feature importance histograms. The error bars represent the standard deviations from 500 independent interrogations for each feature.

at a frequency of 1 Hz, and an irregular waveform [Fig. 3(c)] ranging from 140 to $448\,\mu$ l min $^{-1}$. The control system's working bandwidth is 1.014 Hz, limited by the data acquisition (~0.5 s, averaged over 18 data points) and the syringe pump's response time (~0.5 s). For the step flow, the system effectively reduces the absolute deviation of the actual flow rate from the set flow rate, decreasing from 2%–107% without flow control to 1%–2% with the AI-based flow control. A Fourier analysis of the results for the sinusoidal flow (supplementary material, Fig. S2) shows that our method reduces the deviation from 31% to 2%. For the irregular flow waveform, the deviation is improved from 34% to 7%.

To investigate the robustness of our system to noise, we add artificial random noise with a mean of $-68.66\,\mu$ l min⁻¹ and a standard deviation of $54.38\,\mu$ l min⁻¹ to the sensor output signal for a sinusoidal target waveform ranging between 20 and 320 μ l min⁻¹ before it is fed into the AI controller. As shown in Fig. 3(d), our system maintains flow rate within a narrow range around the target flow rate despite spikes and glitches induced by the noise.

Our findings using the AI-enabled system underscore the accuracy and stability of the closed-loop control of the flow rate of non-Newtonian fluids, as well as its capacity to handle significant sensor signal noise levels. The neural network program effectively addresses

challenges in flow control arising from two sources: the nonlinearity of non-Newtonian fluid flow and the potential for flow-sensing accuracy to be affected by noise. Figure 3(e) shows the permutation feature importance (see the supplementary material—Methods section for details), 27,28 a technique that evaluates the feature importance of each element of the input vector $[r_t, y_t, r_{t-1}, y_{t-1}]$ by randomly shuffling the feature's values and calculating negative mean squared error. Overall, the feature importance values for r and y reflect the nonlinearity and sensing accuracy, respectively, as discussed in the following paragraph.

For the sinusoidal and step waveforms, despite their essential differences, the feature importance values for the four elements are comparable between the two waveforms, with the importance of y higher than that of r. This indicates that for simple waveforms, our cuff-like flow sensor's accuracy is the leading factor in inducing deviations between the controlled flow rate and the target flow rate. The results for the irregular waveform show that the importance of the coulometrically measured flow rate at time t-1 (y_{t-1}) is considerably lower than those of the other three components, reflecting that due to the randomness in the waveform, previous measurement results are less significant. For the sinusoidal waveform with artificial noise, the feature importances of y_t and y_{t-1} are less significant compared to those

of r_t and r_{t-1} , indicating that the superposition of noise to the measured signals reduces the importance of the signal precision.

Our work offers significant promise for applications in additive manufacturing, such as 3D printing, ^{30,31} and in medicine, such as microfluidic biological models.^{25,32} The flow-measurement strategy can be easily integrated into various existing flow-delivering systems. In particular, the contactless method adapts well to dispensing nozzles with different configurations, requiring only a simple process to obtain corresponding calibration curves [such as that shown in Fig. 2(c)]. Additionally, our method quantifies flow velocity without disturbing the flow. These capabilities of our method are difficult for others to match.

See the supplementary material for additional information on the methods, a figure for real-time charge measurement, and a figure for a Fourier analysis of the results for the sinusoidal flow.

J.P. acknowledges support from the NIH NIGMS MIRA (Award No. R35GM151128). J.W.B. acknowledges support from the National Science Foundation CAREER (Award No. CMMI-2047683) and the AFOSR Young Investigator (Award No. FA9550-20-1-0365).

AUTHOR DECLARATIONS Conflict of Interest

The authors have no conflicts to disclose.

Author Contributions

Huilu Bao and Xin Zhang contributed equally to this work.

Huilu Bao: Conceptualization (lead); Formal analysis (lead); Investigation (lead); Methodology (lead); Writing – original draft (lead). Xin Zhang: Conceptualization (lead); Formal analysis (lead); Investigation (lead); Methodology (lead); Writing – original draft (lead). Xiaoyu Zhang: Methodology (supporting); Resources (supporting); Writing – review & editing (supporting). Xiao Fan: Methodology (supporting); Resources (supporting); Writing – review & editing (supporting). J. William Boley: Conceptualization (supporting); Funding acquisition (lead); Resources (supporting); Writing – review & editing (supporting). Jinglei Ping: Conceptualization (lead); Formal analysis (lead); Funding acquisition (lead); Resources (lead); Supervision (lead); Writing – review & editing (lead).

DATA AVAILABILITY

The data that support the findings of this study are available within the article and its supplementary material.

REFERENCES

- ¹N. Shokraneh, M. Alimi, S.-A. Shahidi, M. Mizani, M. Bameni Moghadam, and A. Rafe, "Textural and rheological properties of sliceable ketchup," Gels **9**(3), 222 (2023).
- ²D. M. Prajapati, N. M. Shrigod, R. J. Prajapati, and P. D. Pandit, "Textural and rheological properties of yoghurt: A review," Adv. Life Sci. 5, 5238–5254 (2016).
- ³D. Foresti, K. T. Kroll, R. Amissah, F. Sillani, K. A. Homan, D. Poulikakos, and J. A. Lewis, "Acoustophoretic printing," Sci. Adv. 4(8), eaat1659 (2018).

- ⁴Y. Sun, L. Wang, Y. Ni, H. Zhang, X. Cui, J. Li, Y. Zhu, J. Liu, S. Zhang, Y. Chen, and M. Li, "3D printing of thermosets with diverse rheological and functional applicabilities," Nat. Commun. 14(1), 245 (2023).
- ⁵G. Haghiashtiani, K. Qiu, J. D. Zhingre Sanchez, Z. J. Fuenning, P. Nair, S. E. Ahlberg, P. A. Iaizzo, and M. C. McAlpine, "3D printed patient-specific aortic root models with internal sensors for minimally invasive applications," Sci. Adv. 6(35), eabb4641 (2020).
- ⁶M. Zhou, Z. Qi, Z. Xia, Y. Li, W. Ling, J. Yang, Z. Yang, J. Pei, D. Wu, W. Huo, and X. Huang, "Miniaturized soft centrifugal pumps with magnetic levitation for fluid handling," Sci. Adv. 7(44), eabi7203 (2021).
- for fluid handling," Sci. Adv. 7(44), eabi7203 (2021).

 7R. P. Chhabra, "Non-Newtonian fluids: An introduction," in *Rheology of Complex Fluids*, edited by J. M. Krishnan, A. P. Deshpande, and P. B. S. Kumar (Springer, New York, 2010), pp. 3–34.
- ⁸J. R. Sempionatto, M. Lin, L. Yin, E. De la paz, K. Pei, T. Sonsa-ard, A. N. de Loyola Silva, A. A. Khorshed, F. Zhang, N. Tostado, S. Xu, and J. Wang, "An epidermal patch for the simultaneous monitoring of haemodynamic and metabolic biomarkers," Nat. Biomed. Eng. 5(7), 737–748 (2021).
- ⁹I. Fyrippi, I. Owen, and M. P. Escudier, "Flowmetering of non-Newtonian liquids," Flow Meas. Instrum. 15(3), 131–138 (2004).
- ¹⁰ A. Bista, S. A. Hogan, C. P. O'Donnell, J. T. Tobin, and N. O'Shea, "Evaluation and validation of an inline Coriolis flowmeter to measure dynamic viscosity during laboratory and pilot-scale food processing," Innovative Food Sci. Emerging Technol. 54, 211–218 (2019).
- ¹¹C. Mills, "The consistency of pressure effects between three identical Coriolis flow meters," Flow Meas. Instrum. 80, 102001 (2021).
- ¹²S. Basu, Plant Flow Measurement and Control Handbook (Academic Press, London/Cambridge, MA, 2019).
- ¹³D. A. J. Brion and S. W. Pattinson, "Generalisable 3D printing error detection and correction via multi-head neural networks," Nat. Commun. 13(1), 4654 (2022).
- ¹⁴Y. Ma, J. Potappel, A. Chauhan, M. A. I. Schutyser, R. M. Boom, and L. Zhang, "Improving 3D food printing performance using computer vision and feedforward nozzle motion control," J. Food Eng. 339, 111277 (2023).
- 15 T. J. K. Buchner, S. Rogler, S. Weirich, Y. Armati, B. G. Cangan, J. Ramos, S. T. Twiddy, D. M. Marini, A. Weber, D. Chen, G. Ellson, J. Jacob, W. Zengerle, D. Katalichenko, C. Keny, W. Matusik, and R. K. Katzschmann, "Vision-controlled jetting for composite systems and robots." Nature 623(7987), 522–531 (2023)
- jetting for composite systems and robots," Nature 623(7987), 522–530 (2023).

 16S. Razvarz, C. Vargas-Jarillo, R. Jafari, and A. Gegov, "Flow control of fluid in pipelines using PID controller," IEEE Access 7, 25673–25680 (2019).
- ¹⁷B. Gholami, W. M. Haddad, J. M. Bailey, and W. W. Muir, "Closed-loop control for fluid resuscitation: Recent advances and future challenges," Front. Vet. Sci. 8, 642440 (2021).
- ¹⁸Y. Hu, G. Tang, and D. Huang, "An intelligent control algorithm applied to the flow control of phosphor colloid," in 34th Chinese Control and Decision Conference (CCDC) (IEEE, 2022), pp. 1602–1607.
- ¹⁹G. Fiore, G. Perrino, M. di Bernardo, and D. di Bernardo, "In vivo real-time control of gene expression: A comparative analysis of feedback control strategies in yeast," ACS Synth. Biol. 5(2), 154–162 (2016).
- gies in yeast," ACS Synth. Biol. 5(2), 154–162 (2016).

 20 J.-B. Lugagne, S. Sosa Carrillo, M. Kirch, A. Köhler, G. Batt, and P. Hersen,
 "Balancing a genetic toggle switch by real-time feedback control and periodic forcing," Nat. Commun. 8(1), 1671 (2017).
- ²¹X. Zhang, X. Fan, H. Bao, and J. Ping, "Electrical contactless microfluidic flow quantification," Appl. Phys. Lett. 120(4), 044102 (2022).
- ²²M. Jafari, G. Marquez, J. Selberg, M. Jia, H. Dechiraju, P. Pansodtee, M. Teodorescu, M. Rolandi, and M. Gomez, "Feedback control of bioelectronic devices using machine learning," IEEE Control Syst. Lett. 5(4), 1133–1138 (2021).
- 23). Selberg, M. Jafari, J. Mathews, M. Jia, P. Pansodtee, H. Dechiraju, C. Wu, S. Cordero, A. Flora, N. Yonas, S. Jannetty, M. Diberardinis, M. Teodorescu, M. Levin, M. Gomez, and M. Rolandi, "Machine learning-driven bioelectronics for closed-loop control of cells," Adv. Intell. Syst. 2(12), 2000140 (2020).
- ²⁴K. T. Estelle and B. A. Gozen, "Complex ink flow mechanisms in micro-direct-ink-writing and their implications on flow rate control," Addit. Manuf. 59, 103183 (2022).
- 25 P. L. Mage, B. S. Ferguson, D. Maliniak, K. L. Ploense, T. E. Kippin, and H. T. Soh, "Closed-loop control of circulating drug levels in live animals," Nat. Biomed. Eng. 1(5), 0070 (2017).

- ²⁶J. W. Kopatz, J. Unangst, A. W. Cook, and L. N. Appelhans, "Compositional effects on cure kinetics, mechanical properties and printability of dual-cure epoxy/acrylate resins for DIW additive manufacturing," Addit. Manuf. 46, 102159 (2021).
- ²⁷Y. Ezzyat, P. A. Wanda, D. F. Levy, A. Kadel, A. Aka, I. Pedisich, M. R. Sperling, A. D. Sharan, B. C. Lega, A. Burks, R. E. Gross, C. S. Inman, B. C. Jobst, M. A. Gorenstein, K. A. Davis, G. A. Worrell, M. T. Kucewicz, J. M. Stein, R. Gorniak, S. R. Das, D. S. Rizzuto, and M. J. Kahana, "Closed-loop stimulation of temporal cortex rescues functional networks and improves memory," Nat. Commun. 9(1), 365 (2018).
- ²⁸ K. W. Scangos, A. N. Khambhati, P. M. Daly, G. S. Makhoul, L. P. Sugrue, H. Zamanian, T. X. Liu, V. R. Rao, K. K. Sellers, H. E. Dawes, P. A. Starr,
- A. D. Krystal, and E. F. Chang, "Closed-loop neuromodulation in an individual with treatment-resistant depression," Nat. Med. 27(10), 1696–1700 (2021).
- 29T. Cover and P. Hart, "Nearest neighbor pattern classification," IEEE Trans. Inf. Theory 13(1), 21–27 (1967).
- ³⁰B. Qiu, X. Chen, F. Xu, D. Wu, Y. Zhou, W. Tu, H. Jin, G. He, S. Chen, and D. Sun, "Nanofiber self-consistent additive manufacturing process for 3D microfluidics," Microsyst. Nanoeng. 8(1), 102 (2022).
- 31Y. Liu, Q. Yu, X. Luo, L. Yang, and Y. Cui, "Continuous monitoring of diabetes with an integrated microneedle biosensing device through 3D printing," Microsyst. Nanoeng. 7(1), 75 (2021).
- ³²K. H. K. Wong, J. M. Chan, R. D. Kamm, and J. Tien, "Microfluidic models of vascular functions," Annu. Rev. Biomed. Eng. 14, 205–230 (2012).